PCCP

ROYAL SOCIETY OF CHEMISTRY

PAPER

View Article Online
View Journal | View Issue

Check for updates

Cite this: *Phys. Chem. Chem. Phys.*, 2022, **24**, 17471

Cl-Initiated oxidation of methacrolein under NO_x-free conditions studied by VUV photoionization mass spectrometry†

Xiaoxiao Lin, ‡[a] Rongrong Hu,‡[a] Ziji Ma,[a] Hao Yue,[a] Zuoying Wen,[a] Cuihong Zhang,[ab] Christa Fittschen,[b] Weijun Zhang*[a] and Xiaofeng Tang*[a]

Received 9th May 2022,
Accepted 4th July 2022

DOI: 10.1039/d2cp02101c

rsc.li/pccp

The Cl-initiated oxidation of methacrolein (MACR, C_4H_6O) under NO_x-free conditions has been investigated in a fast flow tube by using a home-made vacuum ultraviolet (VUV) photoionization mass spectrometer complemented by high-level theoretical calculations. The key species such as intermediates and radicals together with products involved in the oxidation are observed online and confirmed in photoionization mass spectra. The reaction potential energy surfaces of the transient C_4H_5O and C_4H_6OCl radicals, formed from the hydrogen-abstraction reaction and the addition reaction of MACR with Cl atoms, with oxygen have been theoretically calculated to illuminate the formation of the peroxy radicals of $C_4H_5OO_2$ and $C_4H_6OClO_2$. The photoionization processes of these peroxy radicals, whose cations are not stable, and their individual self-reactions as well as bimolecular reactions with HO_2 radical are studied and discussed. In addition, kinetic experiments are also performed to get the time evolution of specific products and compared with theoretical models, providing a detailed insight into the reaction mechanism of the Cl-initiated oxidation of MACR.

Published on 05 julio 2022. Downloaded on 4/2/2026 20:38:11.

1. Introduction

Methacrolein (MACR, C_4H_6O) is a key reaction intermediate in atmospheric chemistry and plays an essential role in the atmospheric oxidation of isoprene, the most abundant non-methane volatile organic compound (VOC) in the atmosphere.[1,2] MACR is also an important VOC in the atmosphere and its global emission can approach $\sim$45 Tg year^{-1}.[3] In particular, due to its essential role involved in the oxidation of isoprene, the atmospheric fate of MACR has attracted a great deal of attention in the past decades.[1,4]

The atmospheric fate of MACR is dominated by its reaction with the hydroxyl radical (OH), and mainly proceeds *via* two pathways with approximately equal rates: (i) the addition of OH to the C=C double bond of MACR to generate the OH–MACR adduct radical, and (ii) the abstraction of the aldehyde H-atom to produce the acyl radical, C_4H_5O.[5,6] In the atmosphere, these radicals can react with O_2 and lead to the production of the hydroxyl peroxy radical and the acyl peroxy radical. In addition, these transient peroxy radicals can perform bimolecular reactions with NO_x (NO and NO_2), with themselves or other peroxy radicals (RO_2), with HO_2 or OH radicals depending on the site and time, and contribute to air quality and regional climate.[7–12]

In recent years, researchers found that halogen radicals, particularly chlorine (Cl) atoms formed from photolysis of chlorine (Cl_2), nitrosyl chloride (ClNO), nitryl chloride ($ClNO_2$) and bromine chloride (BrCl), can also have important impacts on the atmospheric degradation of VOCs.[13–16] Among them, Cl atoms can efficiently oxidize VOCs, and the reaction rate constants of Cl atoms with VOCs can be ten times larger than those with OH.[15–18] For example, the reaction rate constant of MACR with Cl atoms was measured at 3.3×10^{-10} cm^3 molecule^{-1} s^{-1}, much larger than that of MACR with OH (3.4×10^{-11} cm^3 molecule^{-1} s^{-1}).[19,20] Therefore, considering the concentrations of OH radicals ($\sim 10^6$ molecules cm^{-3}) and Cl atoms ($\sim 3 \times 10^5$ molecules cm^{-3} during daytime and up to $\sim 8 \times 10^6$ molecules cm^{-3} in the marine boundary layer),[21,22] the Cl-initiated oxidation of MACR can play a significant role in the atmosphere next to that initiated with OH, at least in the marine boundary layer, and has been the subject of experimental and theoretical studies.[20,23]

Similar to the case with the OH radical, the reaction of MACR with Cl atoms can proceed *via* two pathways too: the addition of Cl atom to the C=C bond of MACR to get the

[a] *Laboratory of Atmospheric Physico-Chemistry, Anhui Institute of Optics and Fine Mechanics, HFIPS, Chinese Academy of Sciences, Hefei, 230031 Anhui, China. E-mail: wjzhang@aiofm.ac.cn, tangxf@aiofm.ac.cn*

[b] *University Lille, CNRS, UMR 8522, PC2A – Physicochimie des Processus de Combustion et de l'Atmosphère, F-59000 Lille, France*

† Electronic supplementary information (ESI) available. See DOI: https://doi.org/10.1039/d2cp02101c

‡ These authors contributed equally to this work.

Published on 05 julio 2022. Downloaded on 4/2/2026 20:38:11.

C_4H_6OCl adduct radical, and the hydrogen abstraction to produce the C_4H_5O radical.[19] Previous theoretical calculations show that the Cl-addition to the external carbon of the C=C double bond is the main pathway with a predicted branching ratio of 86%, whereas the branching ratio of the aldehyde-H abstraction is 12% and that of the methyl-H abstraction is 2%.[23]

In the atmosphere, the C_4H_6OCl and C_4H_5O radicals will react with O_2 and the transient peroxy radicals, $C_4H_6OClO_2$ and $C_4H_5OO_2$, can perform various reactions.[11] For example, the peroxy radical $C_4H_6OClO_2$ reacts with itself to form the C_4H_6OClO radical, and its decomposition product, chloroacetone (C_3H_5OCl), was detected with the technique of gas chromatography flame ionization detection (GC-FID).[24] The stable secondary products 2,3-dichloro-2-methylpropanal ($C_4H_6OCl_2$) and methacryloyl chloride (C_4H_5OCl) formed from the reactions of C_4H_6OCl and C_4H_5O radicals with the remaining precursor Cl_2 were also detected in experiments with GC-FID.[25] But, due to the use of online probe techniques to study these reactions, the available information of the Cl-initiated oxidation of MACR is still scarce and the detailed reaction mechanism as well as the formation of the above theoretically proposed key radicals and intermediates needs to be clarified or confirmed.

In this work, the Cl-initiated oxidation reaction of MACR under NO_x-free conditions has been investigated in a fast flow tube reactor by using the online analytical method of vacuum ultraviolet (VUV) photoionization time of flight mass spectrometry complemented by high-level theoretical computations of the structures of radicals and the reaction potential energy surfaces. VUV photoionization mass spectrometry is a powerful analytical method and key species such as radicals and intermediates as well as products involved in the oxidation reactions are directly observed in the experiments.[26,27] The adiabatic ionization energies (AIEs) of these key species are also predicted and utilized to assign the photoionization mass spectra. In addition, to confirm the origins of the products and then to reveal the embedded reaction mechanism, kinetic experiments have also been performed and the time behaviors of products have been obtained and compared with modeling results.

2. Methods

A fast flow tube has been used as a chemical reactor to study the Cl-initiated oxidation reaction of MACR under NO_x-free conditions and a home-made VUV photoionization orthogonal acceleration reflectron time-of-flight (TOF) mass spectrometer is employed to probe and analyze reaction intermediates, radicals and products. The configuration of the fast flow tube and the photoionization mass spectrometer has already been introduced in detail before and so only a brief description is presented here.[28,29]

Briefly, the photoionization mass spectrometer is composed of three vacuum chambers: a source chamber, a photoionization chamber and a TOF chamber. The fast flow tube reactor is installed inside the source chamber and is composed of a 45 cm long Pyrex main tube with a 16/12 mm outer/inner diameter and a 60 cm long coaxial movable injector with a 6/4 mm outer/inner diameter. Cl atoms were generated by microwave discharge (GMS-200W, Sairem) of 1% diluted Cl_2 gas in helium and introduced into the fast flow tube to initiate the oxidation reactions. MACR was introduced through bubbling its liquid at room temperature, and O_2 and helium bath gas were injected *via* the arms of the main tube or the injector. The total pressure inside the flow tube was monitored by a capacity gauge and fixed at 6 Torr by a closed-loop feedback throttle valve. The initial concentrations of MACR, O_2 and Cl atoms in the flow tube were 8×10^{13}, 1×10^{16} and $\sim 1 \times 10^{13}$ molecule cm^{-3}, respectively. Note that the microwave discharge efficiency is not precisely known and so only an estimated concentration of Cl atoms is provided here. The inner surface of the main tube and the outer surface of the injector were coated with halocarbon wax to reduce radical loss on the walls. The reaction time was adjusted by changing the distance between the injector and the sampling skimmer.

After passing through the skimmer (1 mm diameter), the gas mixture from the fast flow tube entered into the photoionization chamber, which was equipped with a commercial Kr discharge lamp (PKS 106, Heraeus) inside. Then the molecules and radicals absorbed the photons of the lamp with energies of $h\nu$ = 10.0 and 10.6 eV, and photoionization processes were induced. A TOF mass analyzer with an orthogonal acceleration and reflectron structure was employed to analyze the masses of ions. The total ion flight length of the TOF mass spectrometer is $\sim$1 m, and its mass resolving power has been measured to be $M/\Delta M \sim 2000$ (FWHM, the full width at half maximum). During the experiments the pressures of the source chamber, the photoionization chamber and the TOF chamber were 800, 1×10^{-2} and 1×10^{-4} Pa, respectively.

High-level theoretical calculations have also been carried out to get the reaction potential energy surfaces, the structures and the ionization energies of radicals and products. Concretely, the potential energy surfaces were calculated for the reactions of C_4H_6OCl and C_4H_5O radicals with O_2 to examine the formation channels leading to the peroxy radicals and other products. The potential energy surfaces were computed at the CCSD(T)-F12a/aug-cc-pVTZ//PBE0/aug-cc-pVDZ level of theory. The structural optimizations and the vibrational frequency calculations were performed with the Gaussian 16 program package.[30] Then the energies of the reactants, the transition states and the products were calculated with the Molpro package.[31] The AIEs of the products were determined from the energy difference of cations and molecules at the PBE0/aug-cc-pVDZ level of theory.

3. Results and discussion

To get detailed information on the reaction system inside the fast flow tube, experiments were performed in sequence and can be divided into two parts.[32,33] Firstly, the experiment was

 This journal is © the Owner Societies 2022

Published on 05 julio 2022. Downloaded on 4/2/2026 20:38:11.

performed without adding oxygen into the fast flow tube, and C_4H_6OCl and C_4H_5O radicals were formed from the Cl-addition reaction and the hydrogen abstraction reaction of MACR with Cl atoms, respectively. Then, with the addition of oxygen, the transient C_4H_6OCl and C_4H_5O radicals reacted with oxygen to produce peroxy radicals and these peroxy radicals could perform self-reactions or react with HO_2 radials in the flow tube under NO_x-free conditions.[11]

3.1 The reaction of MACR with Cl

Without adding oxygen into the fast flow tube, a typical photoionization mass spectrum is presented in Fig. 1(a). Many peaks can be observed in the mass spectrum and the major species have been assigned. The most intense peak at m/z = 70 is ascribed to the reactant MACR itself, whose ionization energy locates at 9.92 eV,[34] below the photon energy of the Kr lamp. The mass peaks at m/z = 69 and m/z = 105/107 should be assigned as C_4H_5O and C_4H_6OCl radicals, respectively, formed from the hydrogen abstraction reaction and the addition reaction of MACR with Cl atoms.[19,23] As far as we known, the transient C_4H_5O and C_4H_6OCl radicals are directly detected here for the first time. The ratio of the mass peaks at m/z = 105 and 107 corresponding to the $C_4H_6O^{35}Cl$ and $C_4H_6O^{37}Cl$ isotopes is measured at ~3, agreeing well with the ratio of the natural abundances of the ^{35}Cl and ^{37}Cl isotopes (100 : 32).[35]

The transient C_4H_5O and C_4H_6OCl radicals can react with the residual Cl_2 molecules in the fast flow tube and the corresponding products have been observed and identified in the mass spectrum, partially with the aid of the isotopic ratio of ^{35}Cl and ^{37}Cl. For example, the mass peaks at m/z = 104 and 106 are assigned as methacryloyl chloride ($C_4H_5O^{35}Cl$ and $C_4H_5O^{37}Cl$), the product of the reaction of C_4H_5O radicals with Cl_2.[25] The small peaks at m/z = 140, 142 and 144 are assigned as 2,3-dichloro-2-methylpropanal ($C_4H_6OCl_2$) from the reaction of C_4H_6OCl radicals with Cl_2.[25] Some products are fragile in the photoionization and their fragment ions have also contributed to the mass spectrum, *i.e.*, at m/z = 76, 78 and 111. The detailed assignment of these peaks and their origins can be found in Table S1 (ESI†).

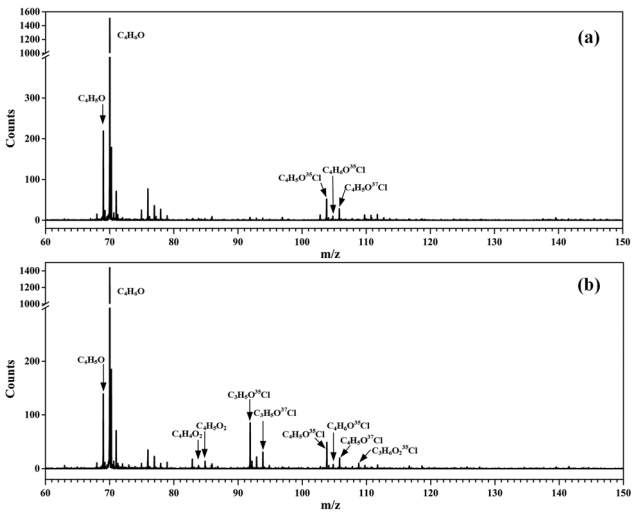

Fig. 1 Photoionization mass spectra acquired (a) without O_2 and (b) adding O_2 into the fast flow tube.

3.2 The reactions of C_4H_5O and C_4H_6OCl with O_2

After adding abundant O_2 (~10^{16} molecule cm^{-3}) into the fast flow tube, the transient C_4H_5O and C_4H_6OCl radicals will mainly react with O_2 and the resulting photoionization mass spectrum is presented in Fig. 1(b). To get a detailed understanding of these processes, the potential energy surfaces (PES) of the reactions of C_4H_5O and C_4H_6OCl radicals with O_2 have been calculated at the CCSD(T)-F12a/aug-cc-pVTZ//PBE0/aug-cc-pVDZ level of theory and are presented in Fig. 2 and 3, respectively, as well as the optimized structures of the species involved in the reactions.

As shown in Fig. 2, the reaction of C_4H_5O with O_2 is an exothermic reaction and the production of the $C_4H_5OO_2$ peroxy radical is energetically favorable. In addition, the theoretical calculations show that the $C_4H_5OO_2$ peroxy radical can perform an H-transfer reaction *via* a transition state (TS) with a submerged barrier of −6.34 kcal mol^{-1} and then dissociate to $C_4H_4O_2$ and OH. The formation of $C_4H_4O_2$ and OH is exothermic with an energy of −39.27 kcal mol^{-1}, indicating that their formation is energetically feasible. As shown in Fig. 1(b), the product $C_4H_4O_2$ has been observed and ascribes to the peak of m/z = 84 in the photoionization mass spectrum.

In Fig. 3, the potential energy surface of the reaction of C_4H_6OCl with O_2 shows that the formation of the $C_4H_6OClO_2$ peroxy radical is also energetically favorable. But, unlike the above case of $C_4H_5OO_2$, the unimolecular reaction of the $C_4H_6OClO_2$ peroxy radical to produce C_4H_5ClO + HO_2 and $C_4H_5ClO_2$ + OH has an energy barrier with a height of 30.09 kcal mol^{-1}, 9.55 kcal mol^{-1} higher than the total energy of C_4H_6OCl with O_2, which is too high to be overcome at room temperature. Thus the $C_4H_6OClO_2$ peroxy radical is the only product in the reaction of C_4H_6OCl with O_2.

As discussed above, the $C_4H_5OO_2$ and $C_4H_6OClO_2$ peroxy radicals are the main products of the reactions of C_4H_5O and

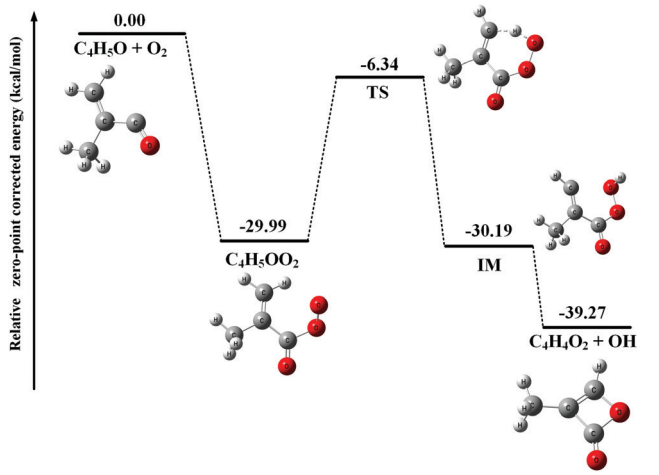

Fig. 2 Potential energy surface of the reaction of C_4H_5O with O_2.

Published on 05 julio 2022. Downloaded on 4/2/2026 20:38:11.

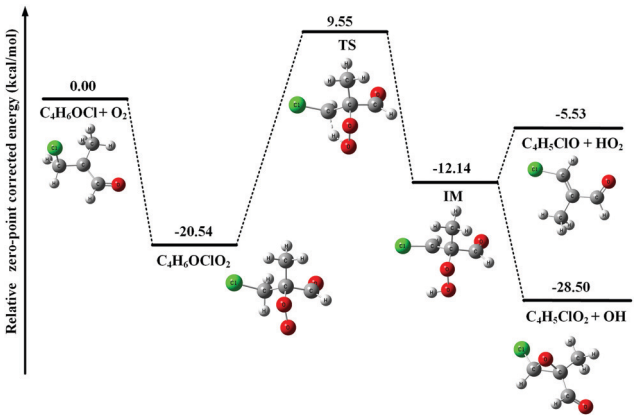

Fig. 3 Potential energy surface of the reaction of C_4H_6OCl with O_2.

C_4H_6OCl radicals with O_2 and their corresponding molecular ions should locate at m/z = 101 and m/z = 137/139, respectively, in the photoionization mass spectrum. However, no such mass peaks can be observed in Fig. 1(b).

Previous studies have shown that except the smallest peroxy radical, CH_3O_2, the cations of most alkyl peroxy radicals are not stable and dissociate to the fragments of alkyl cations and oxygen following the photoionization.[32,33,36] Here, to help to assign the photoionization mass spectrum and to explain the dissociative photoionization processes of the $C_4H_5OO_2$ and $C_4H_6OClO_2$ peroxy radicals, theoretical calculations have also been performed. Fig. 4 presents the optimized structures of the $C_4H_5OO_2$ and $C_4H_6OClO_2$ peroxy radicals and their cations in the ground electronic state. The ground electronic state of these cations is a triplet state after removing an electron from the σ(Cα-OO) orbital of the $C_4H_5OO_2$ and $C_4H_6OClO_2$ peroxy radicals. To be specific, the C–OO equilibrium bond length of the neutral $C_4H_6OClO_2$ is calculated at 1.450 Å, whereas it is substantially elongated to 2.781 Å for the cationic ground

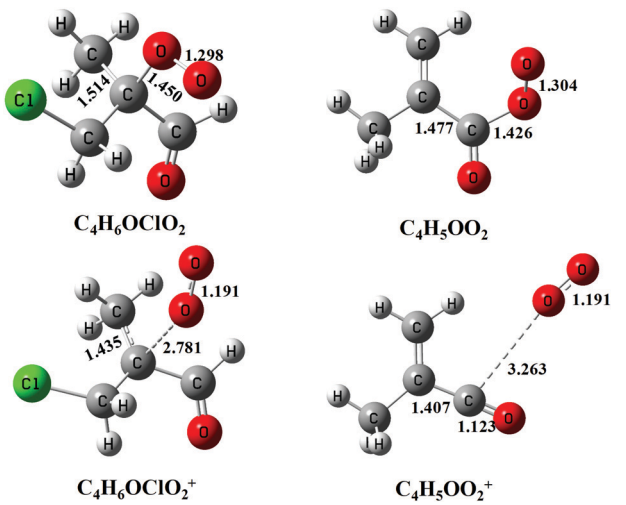

Fig. 4 The structures of the $C_4H_6OClO_2$ and $C_4H_5OO_2$ peroxy radicals and their cations optimized at the PBE0/aug-cc-pVDZ level of theory. The bond lengths are in Å.

electronic state of $C_4H_6OClO_2^+$. Similarly, the C–OO bond length of $C_4H_5OO_2^+$ at the ground electronic state is also elongated from 1.426 to 3.263 Å during photoionization.[27,33]

These apparent elongations of the C–OO bond length will reduce the stability of the peroxy radicals' cations, also making $C_4H_5OO_2^+$ and $C_4H_6OClO_2^+$ only slightly bound and out of the Franck–Condon transition during photoionization.[27,33] In addition, the AIEs of the $C_4H_5OO_2$ and $C_4H_6OClO_2$ peroxy radicals are calculated and take the values of 7.93 and 9.23 eV, respectively, far below the present photon energy of 10.6 eV. The appearance energies (AEs) of the fragment ions $C_4H_5O^+$ (m/z = 69) and $C_4H_6OCl^+$ (m/z = 105/107) in the dissociation of $C_4H_5OO_2^+$ and $C_4H_6OClO_2^+$ are also calculated and locate at 8.00 and 9.08 eV. Therefore, in the photoionization the $C_4H_5OO_2^+$ and $C_4H_6OClO_2^+$ cations will be produced with a high internal energy and dissociate to the $C_4H_5O^+ + O_2$ and $C_4H_6OCl^+ + O_2$ fragments, respectively. Thus, the mass peak at m/z = 69 ($C_4H_5O^+$) in Fig. 1(b) is attributed to $C_4H_5OO_2$, and the mass peaks at m/z = 105/107 ($C_4H_6OCl^+$) is ascribed to the $C_4H_6OClO_2$ peroxy radical.

3.3 The reactions of $C_4H_5OO_2$ and $C_4H_6OClO_2$ under NO_x free conditions

Under NO_x free conditions in the fast flow tube, the $C_4H_5OO_2$ and $C_4H_6OClO_2$ peroxy radicals can perform self-reaction or react with HO_2 radicals.[11] Normally, the self-reaction of peroxy radicals (RO_2) has two channels, (i) $2RO_2 \rightarrow 2RO + O_2$ and (ii) $2RO_2 \rightarrow R\_HO + ROH + O_2$.[37] But, based on the specific structures of $C_4H_5OO_2$ and $C_4H_6OClO_2$, as shown in Fig. 4, there are no H atoms on the tertiary α-oxyl carbon to be abstracted and thus the self-reactions of $C_4H_5OO_2$ and $C_4H_6OClO_2$ do not proceed *via* channel (ii).[38]

Normally the reaction of the alkoxy radical RO with O_2 is one of the major sources to produce HO_2 radicals. But, the reaction of C_4H_5O with O_2 will not produce HO_2, as still there is no H atoms on the tertiary α-oxyl carbon to be abstracted. A previous study shows that the reaction of C_4H_6OClO with O_2 can generate HO_2, *via* more than one elementary reaction step,[39] and presently this reaction should be the main source of HO_2 in the fast flow tube. Note that the AIE of HO_2 locates at 11.359 eV, above the present photon energy, and thus no HO_2 radicals can be observed in the mass spectra.[40]

A previous study predicts that the reaction of the $C_4H_5OO_2$ peroxy radical with HO_2 has three channels, (R1a) $C_4H_5OO_2 + HO_2 \rightarrow C_4H_5OO_2H + O_2$, (R1b) $C_4H_5OO_2 + HO_2 \rightarrow C_4H_5OOH + O_3$, and (R1c) $C_4H_5OO_2 + HO_2 \rightarrow C_4H_5OO + OH + O_2$.[39] The reaction of $C_4H_6OClO_2$ with HO_2 has two channels, (R2a) $C_4H_6OClO_2 + HO_2 \rightarrow C_4H_6OClOOH + O_2$, (R2b) $C_4H_6OClO_2 + HO_2 \rightarrow C_4H_6OClO + OH + O_2$, and the branching ratio was predicted at $Y_{R2a} = 0.2 \pm 0.2$ and $Y_{R2b} = 0.8 \pm 0.2$.[39]

The alkoxy radical C_4H_6OClO formed from the self-reaction of $C_4H_6OClO_2$ or its bimolecular reaction with HO_2 can decompose to the stable product of chloroacetone ($C_3H_5O^{35}Cl$ and $C_3H_5O^{37}Cl$) with a fast rate of $\sim 10^7$ s^{-1} and has been completely consumed in the fast flow tube within the reaction time of ~1 ms under the present experimental conditions.[39] Therefore,

 This journal is © the Owner Societies 2022

Published on 05 julio 2022. Downloaded on 4/2/2026 20:38:11.

the signal of C_4H_6OClO (m/z = 121) is not observed in the photoionization mass spectrum of Fig. 1(b), and its decomposition product of chloroacetone (C_3H_5OCl) contributes to the mass peaks of m/z = 92 and 94 with a ratio of 3 : 1.

The reaction of $C_4H_6OClO_2$ with HO_2 can produce the hydroperoxide $C_4H_6OClOOH$ (m/z = 138, 140). The AIE of $C_4H_6OClOOH$ is calculated at 9.30 eV at the PBE0/aug-cc-pVDZ level of theory, and the appearance energy of its fragment ion $C_3H_5ClO_2H^+$ is predicted at 9.97 eV. Thus in the photoionization the hydroperoxide cation $C_4H_6OClOOH^+$ is produced with a high internal energy and dissociates into the fragment ion of $C_3H_5ClOOH^+$, plus the neutral fragment of CHO, contributing to the peaks of m/z = 109 and 111 in the photoionization mass spectrum of Fig. 1(b).

The peroxy radical of $C_4H_5OO_2$ performs self-reaction and reacts with HO_2 to generate the radical C_4H_5OO, contributing to the mass peak of m/z = 85 in Fig. 1(b). The reaction of $C_4H_5OO_2$ with HO_2 can also produce C_4H_5OOH (m/z = 86) and $C_4H_5OO_2H$ (m/z = 102). The AIE of $C_4H_5OO_2H$ is calculated at 9.44 eV at the PBE0/aug-cc-pVDZ level of theory. In the photoionization, the $C_4H_5OO_2H^+$ cation was produced with a high internal energy and then dissociated into the $C_4H_5O^+$ (m/z = 69) and HO_2 fragments.

3.4 Reaction mechanism

Kinetic experiments have been performed for the Cl-initiated oxidation reaction of MACR by changing the distance between the injector and the sampling skimmer, to get information inside the fast flow tube and to confirm the above species' assignments.[28,29] The time evolution of ion signals has been measured and some of them, *i.e.* m/z = 84, 85 and 92 corresponding to $C_4H_4O_2$, C_4H_5OO and C_3H_5OCl, are presented in Fig. 5. In addition, the time evolutions of the species' concentrations have been theoretically calculated based on the oxidation reactions listed in Table 1 and are presented as solid lines,

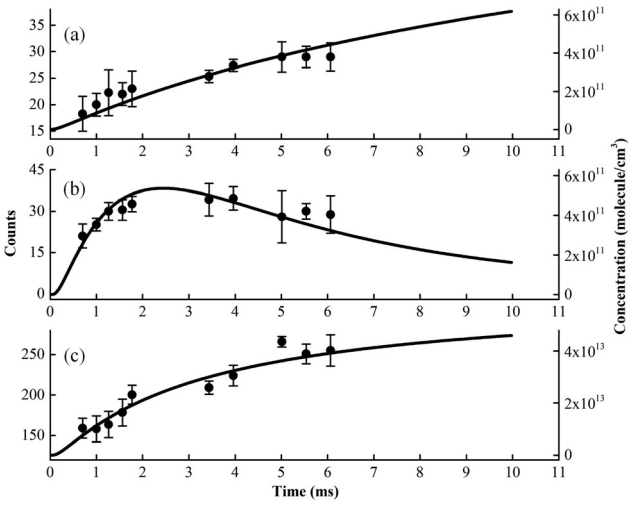

Fig. 5 The experimental (dots) and theoretical (lines) time behavior of products in the Cl-initiated oxidation of MACR. (a) m/z = 84, (b) m/z = 85 and (c) m/z = 92.

Table 1 Reaction mechanism used to model experiments in this work

	Reaction	Rate coefficient/cm^3 molecule^{-1} s^{-1} or s^{-1}	Ref.
1	$C_4H_6O + Cl \rightarrow C_4H_6OCl$	1.98×10^{-10}	23
2	$C_4H_6O + Cl \rightarrow C_4H_5O + HCl$	2.76×10^{-11}	23
3	$C_4H_6OCl + O_2 \rightarrow C_4H_6OClO_2$	2.87×10^{-12}	43
4	$C_4H_5O + O_2 \rightarrow C_4H_5OO_2$	2.0×10^{-12}	44
5	$C_4H_5OO_2 \rightarrow C_4H_4O_2 + OH$	12.9[a]	45
6	$2C_4H_6OClO_2 \rightarrow 2C_4H_6OClO + O_2$	2.4×10^{-12}	39
7	$2C_4H_5OO_2 \rightarrow 2C_4H_5OO + O_2$	1.0×10^{-11}	39
8(a)	$C_4H_6OClO_2 + HO_2 \rightarrow C_4H_6OClO_2H + O_2$	2.0×10^{-12}	39
8(b)	$C_4H_6OClO_2 + HO_2 \rightarrow C_4H_6OClO + OH + O_2$	8.0×10^{-12}	39
9(a)	$C_4H_5OO_2 + HO_2 \rightarrow C_4H_5OO_2H + O_2$	7.7×10^{-12}	39
9(b)	$C_4H_5OO_2 + HO_2 \rightarrow C_4H_5OOH + O_3$	5.5×10^{-12}	39
9(c)	$C_4H_5OO_2 + HO_2 \rightarrow C_4H_5OO + OH + O_2$	8.8×10^{-12}	39
10	$C_4H_6OClO\ (+O_2) \rightarrow C_3H_5OCl + HO_2 + CO$	1×10^{7}[b]	39
11	$C_4H_5OO \rightarrow C_3H_5 + CO_2$	7×10^{2}	46
12	$2HO_2 \rightarrow H_2O_2 + O_2$	1.7×10^{-12}	47
13	$HO_2 \rightarrow$ diffusion	3	41

[a] Analogic result from ref. 45. [b] The reaction consists of more than one elementary reaction step, seen the detail in ref. 39.

also seen in Fig. S1 and S2 (ESI†).[41,42] Note that the experimental concentration equivalents are less well-defined, as some unknown and conversion factors such as photoionization cross-sections add to the measurement uncertainty. The theoretical results also rely on a number of assumptions, for instance, the initial concentration of Cl atoms and the unknown or estimated rate constants. As shown in Fig. 5, although with some differences, the overall shape of the theoretical modeling results can compare with the time evolution of the ion signals.

We can see that the ion signal of m/z = 84 increases with time within the experimentally covered time region, which is consistent with the theoretically modeled time behavior of $C_4H_4O_2$ in Fig. 5(a). The signal intensity at m/z = 85 firstly increases and then decreases with time, which is a typical radical behavior of C_4H_5OO, as shown in Fig. 5(b). The signal of m/z = 92 firstly increases and then stabilizes, which is in agreement with the expected time behavior of chloroacetone. The detailed reaction mechanism of the Cl-initiated oxidation of MACR under NO_x free conditions has been summarized in Fig. 6. Note that Fig. 6 only presents the two dominant entrance channels for the reaction of MACR with Cl atoms, the terminal addition of the C=C double bond and the aldehyde-H abstraction with their branching ratios of about 86% and 12%, respectively.[39] The branching ratio of the minor methyl-H abstraction channel is predicted at only 2%, not shown in Fig. 6, and this isomeric production channel is difficult to be separated only with the fixed-photon-energy photoionization mass spectrometry.

4. Conclusions

In summary, we present here a combined experimental and theoretical study on the Cl-initiated oxidation of MACR under

Published on 05 julio 2022. Downloaded on 4/2/2026 20:38:11.

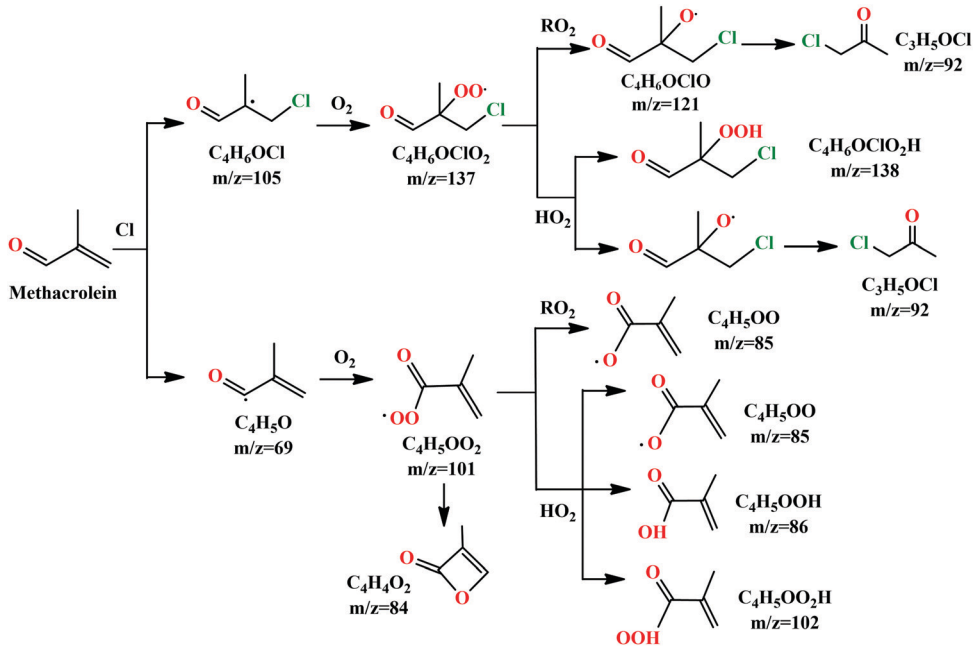

Fig. 6 Reaction mechanisms of Cl-initiated oxidation of MACR under NO_x free conditions.

NO_x-free conditions. A microwave discharge fast flow tube was used to investigate the oxidation reaction of MACR. The reaction products and the key intermediates as well as radicals have been observed online by using a home-made VUV photoionization mass spectrometer. It is shown that the reaction of MACR with Cl atoms can proceed *via* two pathways, the addition of Cl atom to the C=C double bond of MACR to produce the C_4H_6OCl adduct radical and the abstraction of the aldehyde hydrogen atom to produce the C_4H_5O radical. These radicals can react with oxygen to produce their corresponding peroxy radicals, whose photoionization processes have also been discussed and utilized to assign the photoionization mass spectra. The transient C_4H_5O and C_4H_6OCl radicals, as well as the peroxy radicals $C_4H_5OO_2$ and $C_4H_6OClO_2$, are experimentally detected here for the first time, directly confirming the above reaction mechanisms. Under NO_x-free conditions, these peroxy radicals will perform self-reaction and react with HO_2 radicals. The resulting specific products are clearly identified in the photoionization mass spectra too, with the aid of theoretical calculations. In addition, the time evolutions of products have been measured in the kinetic experiments and compared with theoretically modeled results. The present work provides a detailed insight into the reaction mechanisms of the Cl-initiated oxidation of MACR and will be helpful to understand the atmospheric fate of MACR.

Author contributions

Xiaoxiao Lin: conceptualization, formal analysis, investigation, writing – original draft. Rongrong Hu: investigation, writing – original draft. Ziji Ma: investigation. Hao Yue: investigation. Zuoying Wen: investigation. Cuihong Zhang: investigation. Christa Fittschen: writing – review & editing. Weijun Zhang: investigation. Xiaofeng Tang: conceptualization, methodology, investigation, funding acquisition, project administration, writing – review & editing.

Conflicts of interest

There are no conflicts to declare.

Acknowledgements

This work was financially supported by the National Natural Science Foundation of China (No. 42075113, 91961123, 42120104007), the International Partnership Program of Chinese Academy of Sciences (No. 116134KYSB20170048) and the Key Program of Research and Development of Hefei Science Center, CAS (No. 2020HSCKPRD001).

References

1 P. O. Wennberg, K. H. Bates, J. D. Crounse, L. G. Dodson and R. C. McVay, *et al.*, Gas-phase reactions of isoprene and its major oxidation products, *Chem. Rev.*, 2018, **118**, 3337–3390.
2 X. Wang, J. Sun, L. Bao, Q. Mei and B. Wei, *et al.*, Mechanisms and kinetic parameters for the gas-phase reactions of 3-methyl-3-buten-2-one and 3-methyl-3-penten-2-one with ozone, *J. Phys. Chem. A*, 2019, **123**, 2745–2755.
3 J. D. Crounse, F. Paulot, H. G. Kjaergaard and P. O. Wennberg, Peroxy radical isomerization in the oxidation of isoprene, *Phys. Chem. Chem. Phys.*, 2011, **13**, 13607–13613.

 This journal is © the Owner Societies 2022

Published on 05 julio 2022. Downloaded on 4/2/2026 20:38:11.

4 T. Gierczak, J. B. Burkholder, R. K. Talukdar, A. Mellouki and S. Barone, *et al.*, Atmospheric fate of methyl vinyl ketone and methacrolein, *J. Photochem. Photobiol., A*, 1997, **110**, 1–10.
5 H. G. Kjaergaard, H. C. Knap, K. B. Ørnsø, S. Jørgensen and J. D. Crounse, *et al.*, Atmospheric fate of methacrolein. 2. Formation of lactone and implications for organic aerosol production, *J. Phys. Chem. A*, 2012, **116**, 5763–5768.
6 J. J. Orlando, G. S. Tyndall and S. E. Paulson, Mechanism of the OH-initiated oxidation of methacrolein, *Geophys. Res. Lett.*, 1999, **26**, 2191–2194.
7 M. Claeys, W. Wang, A. C. Ion, I. Kourtchev and A. Gelencsér, *et al.*, Formation of secondary organic aerosols from isoprene and its gas-phase oxidation products through reaction with hydrogen peroxide, *Atmos. Environ.*, 2004, **38**, 4093–4098.
8 Z. Chen, H. Wang, L. Zhu, C. Wang and C. Jie, *et al.*, Aqueous-phase ozonolysis of methacrolein and methyl vinyl ketone: A potentially important source of atmospheric aqueous oxidants, *Atmos. Chem. Phys.*, 2008, **8**, 2255–2265.
9 Y. Liu, F. Siekmann, P. Renard, A. El Zein and G. Salque, *et al.*, Oligomer and SOA formation through aqueous phase photooxidation of methacrolein and methyl vinyl ketone, *Atmos. Environ.*, 2012, **49**, 123–129.
10 X. Zhang, Z. Chen and Y. Zhao, Laboratory simulation for the aqueous OH-oxidation of methyl vinyl ketone and methacrolein: Significance to the in-cloud SOA production, *Atmos. Chem. Phys.*, 2010, **10**, 9551–9561.
11 J. J. Orlando and G. S. Tyndall, Laboratory studies of organic peroxy radical chemistry: An overview with emphasis on recent issues of atmospheric significance, *Chem. Soc. Rev.*, 2012, **41**, 6294–6317.
12 C. Fittschen, The reaction of peroxy radicals with OH radicals, *Chem. Phys. Lett.*, 2019, **725**, 102–108.
13 T. Sherwen, M. J. Evans, R. Sommariva, L. D. Hollis and S. M. Ball, *et al.*, Effects of halogens on European air-quality, *Faraday Discuss.*, 2017, **200**, 75–100.
14 W. R. Simpson, S. S. Brown, A. Saiz-Lopez, J. A. Thornton and R. von Glasow, Tropospheric halogen chemistry: Sources, cycling, and impacts, *Chem. Rev.*, 2015, **115**, 4035–4062.
15 R. Gao, L. Zhu, Q. Zhang and W. Wang, Atmospheric oxidation mechanism and kinetic studies for OH and NO_3 radical-initiated reaction of methyl methacrylate, *Int. J. Mol. Sci.*, 2014, **15**, 5032–5044.
16 M. Lawler, R. Sander, L. Carpenter, J. Lee and R. v Glasow, *et al.*, HOCl and Cl_2 observations in marine air, *Atmos. Chem. Phys.*, 2011, **11**, 7617–7628.
17 Y. Sun, Q. Zhang, J. Hu, J. Chen and W. Wang, Theoretical study for OH radical-initiated atmospheric oxidation of ethyl acrylate, *Chemosphere*, 2015, **119**, 626–633.
18 X. Liu, H. Qu, L. G. Huey, Y. Wang and S. Sjostedt, *et al.*, High levels of daytime molecular chlorine and nitryl chloride at a rural site on the north China plain, *Environ. Sci. Technol.*, 2017, **51**, 9588–9595.
19 C. E. Canosa-Mas, E. S. N. Cotter, J. Duffy, K. C. Thompson and R. P. Wayne, The reactions of atomic chlorine with acrolein, methacrolein and methyl vinyl ketone, *Phys. Chem. Chem. Phys.*, 2001, **3**, 3075–3084.
20 W. H. Wang, M. J. Ezell, A. A. Ezell, G. Soskin and B. J. Finlayson, Rate constants for the reactions of chlorine atoms with a series of unsaturated aldehydes and ketones at 298 K: Structure and reactivity, *Phys. Chem. Chem. Phys.*, 2002, **4**, 1824–1831.
21 C.-T. Chang, T.-H. Liu and F.-T. Jeng, Atmospheric concentrations of the Cl atom, CIO radical, and HO radical in the coastal marine boundary layer, *Environ. Res.*, 2004, **94**, 67–74.
22 C. Mallik, L. Tomsche, E. Bourtsoukidis, J. N. Crowley and B. Derstroff, *et al.*, Oxidation processes in the eastern Mediterranean atmosphere: Evidence from the modelling of HO_x measurements over Cyprus, *Atmos. Chem. Phys.*, 2018, **18**, 10825–10847.
23 C. Sun, B. Xu and S. Zhang, Atmospheric reaction of Cl^+ methacrolein: A theoretical study on the mechanism, and pressure-and temperature-dependent rate constants, *J. Phys. Chem. A*, 2014, **118**, 3541–3551.
24 J. J. Orlando, G. S. Tyndall, E. C. Apel, D. D. Riemer and S. E. Paulson, Rate coefficients and mechanisms of the reaction of Cl-atoms with a series of unsaturated hydrocarbons under atmospheric conditions, *Int. J. Chem. Kinet.*, 2003, **35**, 334–353.
25 E. W. Kaiser, I. R. Pala and T. J. Wallington, Kinetics and mechanism of the reaction of methacrolein with chlorine atoms in 1–950 torr of N_2 or N_2/O_2 diluent at 297 K, *J. Phys. Chem. A*, 2010, **114**, 6850–6860.
26 X. Lin, X. Tang, Z. Wen, B. Long and C. Fittschen, *et al.*, Direct observation of the particle-phase bicyclic products from OH-initiated oxidation of 1,3,5-trimethylbenzene under NO_x-free conditions, *Atmos. Environ.*, 2022, **271**, 118914.
27 X. Tang, X. Lin, G. A. Garcia, J.-C. Loison and Z. Gouid, *et al.*, Identifying isomers of peroxy radicals in the gas phase: 1-$C_3H_7O_2$ *vs.* 2-$C_3H_7O_2$., *Chem. Commun.*, 2020, **56**, 15525–15528.
28 Z. Wen, X. Tang, C. Fittschen, C. Zhang and T. Wang, *et al.*, Online analysis of gas-phase radical reactions using vacuum ultraviolet lamp photoionization and time-of-flight mass spectrometry, *Rev. Sci. Instrum.*, 2020, **91**, 043201.
29 Z. Wen, X. Tang, C. Wang, C. Fittschen and T. Wang, *et al.*, A vacuum ultraviolet photoionization time-of-flight mass spectrometer with high sensitivity for study of gas-phase radical reaction in a flow tube, *Int. J. Chem. Kinet.*, 2019, **51**, 178–188.
30 M. Frisch, G. Trucks, H. Schlegel, G. Scuseria and M. Robb, *et al.*, *Gaussian 16 revision a.03. 2016*, Gaussian Inc., 2016.
31 H. J. Werner and P. J. Knowles, *Getting started with Molpro version 2015.1*, 2015.
32 X. Tang, X. Gu, X. Lin, W. Zhang and G. A. Garcia, *et al.*, Vacuum ultraviolet photodynamics of the methyl peroxy radical studied by double imaging photoelectron photoion coincidences, *J. Chem. Phys.*, 2020, **152**, 104301.
33 Z. Wen, X. Lin, X. Tang, B. Long and C. Wang, *et al.*, Vacuum ultraviolet photochemistry of the conformers of the ethyl

Published on 05 julio 2022. Downloaded on 4/2/2026 20:38:11.

peroxy radical, *Phys. Chem. Chem. Phys.*, 2021, **23**, 22096–22102.
34 NIST Chemistry WebBook, 2022, **https://webbook.nist.gov/chemistry/**.
35 K. J. R. Rosman and P. D. P. Taylor, Isotopic compositions of the elements 1997, *J. Anal. At. Spectrom.*, 1999, **14**, 5N–24N.
36 G. Meloni, P. Zou, S. J. Klippenstein, M. Ahmed and S. R. Leone, *et al.*, Energy-resolved photoionization of alkylperoxy radicals and the stability of their cations, *J. Am. Chem. Soc.*, 2006, **128**, 13559–13567.
37 D. M. Rowley, P. D. Lightfoot, R. Lesclaux and T. J. Wallington, Ultraviolet absorption spectrum and self-reaction of cyclopentylperoxy radicals, *J. Chem. Soc., Faraday Trans.*, 1992, **88**, 1369–1376.
38 G. Hasan, R. R. Valiev, V.-T. Salo and T. Kurtén, Computational investigation of the formation of peroxide (ROOR) accretion products in the OH- and NO_3-initiated oxidation of α-pinene, *J. Phys. Chem. A*, 2021, **125**, 10632–10639.
39 A. S. Hasson, G. S. Tyndall, J. J. Orlando, S. Singh and S. Q. Hernandez, *et al.*, Branching ratios for the reaction of selected carbonyl-containing peroxy radicals with hydroperoxy radicals, *J. Phys. Chem. A*, 2012, **116**, 6264–6281.
40 X. Tang, X. Lin, G. A. Garcia, J.-C. Loison and C. Fittschen, *et al.*, Threshold photoelectron spectroscopy of the HO_2 radical, *J. Chem. Phys.*, 2020, **153**, 124306.
41 C. Zhang, M. Shamas, M. Assali, X. Tang and W. Zhang, *et al.*, Absolute absorption cross-section of the $\tilde{A} \leftarrow \tilde{X}$ electronic transition of the ethyl peroxy radical and rate constant of its cross reaction with HO_2, *Photonics*, 2021, **8**, 296.
42 M. Shamas, M. Assali, C. Zhang, X. Tang and W. Zhang, *et al.*, Rate constant and branching ratio for the reactions of the ethyl peroxy radical with ttself and with the ethoxy radical, *ACS Earth Space Chem.*, 2021, **6**, 181–188.
43 J. D. DeSain, S. J. Klippenstein, J. A. Miller and C. A. Taatjes, Measurements, theory, and modeling of OH formation in ethyl + O_2 and propyl + O_2 reactions, *J. Phys. Chem. A*, 2003, **107**, 4415–4427.
44 C. E. Mcdade, T. M. Lenhardt and K. D. Bayers, The rate of reaction of acetyl and benzoyl radicals with O_2, *J. Photochem.*, 1982, **20**, 1–7.
45 F. Zhang and T. S. Dibble, Effects of olefin group and its position on the kinetics for intramolecular H-shift and HO_2 elimination of alkenyl peroxy radicals, *J. Phys. Chem. A*, 2011, **115**, 655–663.
46 H. Ning, J. Wu, L. Ma, W. Ren and D. F. Davidson, *et al.*, Combined ab initio, kinetic modeling, and shock tube study of the thermal decomposition of ethyl formate, *J. Phys. Chem. A*, 2017, **121**, 6568–6579.
47 W. DeMoore, S. Sander and D. Golden, *JPL Publication 97-4*, Institute of Technology, 1997.

 This journal is © the Owner Societies 2022